Journal of Micro-Bio Robotics (2018) 14:41–49
https://doi.org/10.1007/s12213-018-0107-0

RESEARCH PAPER

Motion planning of particle based microrobots for static obstacle avoidance

Hoyeon Kim[1] · U. Kei Cheang[2] · Louis W. Rogowski[1] · Min Jun Kim[1]

Received: 26 February 2018 / Revised: 23 April 2018 / Accepted: 2 May 2018 / Published online: 12 May 2018

Abstract

Magnetic microrobots have been shown to be effective at navigating microscale environments which has led to many investigations reguarding the motion control of microrobots. To increase the feasibility of using microrobots for microscale tasks and widen the range of potential applications, the use of autonomous navigation systems will be essential. In this work, the magnetic particle based achiral microrobots are controlled wirelessly using a combination of rotating and static magnetic fields generated from electromagnetic coils in an approximate Helmholtz configuration. In previous work, we developed both a kinematic model for particle based microrobots and a feedback controller; once implemented, the controller can guide the microrobots to any goal positions. In the present work, we demonstrate path planning motion control for magnetic particle based microrobots in microfluidic channels formed using patterned static SU-8 microstructures. The microrobots were able to avoid collision with the microstructures, which acted as static obstacles, by using a gradient path method. In experiments, microrobots were able to reach the final goal position by following waypoints of generated path from the gradient path method in a static obstacle laden environment.

Keywords Microrobot · Magnetic control · Obstacle avoidance · Path planning

1 Introduction

The application of microrobotics for cell manipulation, microassembly, drug delivery, and so on, hinges on the ability to implement motion control and manipulation in low Reynolds number environments. At low Reynolds number, as a result of their small sizes and velocities, microrobots in motion are subjected to negligible inertial effects and are dominated by viscous forces. Therefore, microrobots must generate nonreciprocal motions for swimming [1]. To generate such motions, most previously developed microrobots have been inspired by the scallop theorem [1] and generate propulsive force using chirality or flexibility [2–8]. Other examples include magnetically steered swimming cells [9], electrically-controlled bacterial microrobots [10], optically- deformed 3-bead systems [11], and biflagellate micro-objects [12]. For controlling microrobots, magnetic actuation has shown to be the most effective method due to the ease of transferring power over long range with minimal health effects. There are various examples of magnetic actuation for biomimetic and non-biomimetic microrobots [13, 14]. Most microrobot designs are based on torque-driven actuation using rotating magnetic fields [13] while other cases used magnetic force-driven actuation [15–17]. In this paper, magnetic particle based microrobots were used. Actuated from the magnetic torque generated a rotating magnetic field, these microrobots can swim in low Reynolds number environments controlled in terms of velocity and direction.

In order to demonstrate the feasibility to use microrobots for practical application, it is important to strengthen the navigation capability of microrobots. For navigating in narrow paths or confined spaces, an autonomous navigation system is required to provide reliable path planning and motion control [18–20]. This integral autonomous control system can help microrobots perform microscale tasks such as cell

Hoyeon Kim and U. Kei Cheang contributed equally to this work.

Electronic supplementary material The online version of this article (https://doi.org/10.1007/s12213-018-0107-0) contains supplementary material, which is available to authorized users.

✉ Min Jun Kim
mjkim@lyle.smu.edu

[1] Department of Mechanical Engineering, Southern Methodist University, Dallas, TX 75275, USA

[2] Department of Mechanical and Energy Engineering, Southern University of Science and Technology, Shenzhen 518055, Guangdong, China

manipulation, cell sorting, cell fusion, and microassembly. Originally, there had been a few works on automatic manipulation using path planning with optical tweezers [21–24]. The Rapidly-exploring random trees (RRT) method has been applied to optical tweezers for robotic manipulation of biological cells [24]. Also, micromanipulation has been utilized with A* algorithm for microassembly work [25]. Recently, autonomous navigation algorithms have been utilized for an untethered microrobot [26–29] and various path planners are compared in terms of computation time, trajectory length, and elapsed time [30]. Magnetotactic *T. pyriformis* was guided by implementation of RRT path planning [27], and the predefined path was generated for microrobots by fast marching methods (FMM) using the captured MRI image [26]. For rolling microrobots [28], model predictive control (MPC) was applied to supply the path, taking into consideration the kinematic constraints, by solving an optimization problem over a finite time [29]. On the other hand, lattice-based planning using a search-based planning library (SB PL) was used for the same robot and the microrobot followed the path [28]. Most of these approaches are based on nonholonomic and kinematic constraints of the microrobots, due to the design of the microrobot and the actuation method similar with mobile robots [31, 32]. In addition, there had not been lots of research that were implemented in real experimental environments; rather, they were simulated using real image that was obtained by MRI or an image processing camera [33]. Some of these methods were implemented in real experimental environments; such as, liquid environment containing crystals [28, 34]. Therefore, path planning and motion control are required to be performed under environmental constraints; such as, limited free space due to large area occupied by obstacles. Herein, the aim of our work is to demonstrate the path planning and motion control for approaching the goal position by passing between static obstacles.

The proposed path planning in this work demonstrates the ability to guide a microrobot through confined and narrow spaces in real time, which is essential for minimally invasive procedures and intravascular therapy. A control system with a combination of path planning and real time motion control allows an untethered microrobot to follow a predefined path with high reliability and safety. We fabricated the static obstacles using traditional photolithography processes. We then fabricated the achiral microrobots; which consist of magnetic particles that are held together through strongly bonded chemical bindings and magnetic forces. Upon actuation via a rotating magnetic field, the microrobots convert rotation motion into translation motion. In previous work, it was demonstrated that combining a rotating magnetic field, which actuates microrobots to swim, and a static magnetic field, which maintains the orientation of the microrobots [35], is an effective control method. Kinematic model and a feedback control law for our microrobots were investigated in Ref. [29, 34]. In this paper, we utilized a gradient path planning method [36] and demonstrated the trajectory tracking of the microrobots in fluid environments occupied by static obstacles. In addition, different microrobots that had different number of particles were applied to the experimental chambers, where obstacles of different sizes and shapes were placed. Photolithography was used to fabricate the static obstacles which have a height of 260 μm. To reach the waypoints of gradient path planning, a nonlinear feedback controller [35] was adapted to guide the particle based microrobots. As a result, the microrobots successfully reached the goal position with minimal error when compared to the generated path. The main objective of this paper is to demonstrate the use of a path planner to safely navigate achiral microrobots to reach the goal position without collision with big static obstacles.

The paper is organized as follows: Section 2 introduces the fabrication and actuation method of the particle based microrobots. In section 3, the kinematic model of microrobots and motion control are presented, and the application of path planning is described. At last, the implemented experimental results in two different environments are explained in section 4.

2 Particle based microrobots

2.1 Fabrication and actuation of particle based microrobots

Our particle based microrobot consists of multiple magnetic particles, each with a diameter of 4.35 μm. The magnetic beads are bonded together by chemical and innate magnetic attraction forces. Biotin and avidin coated particles are assembled in a chain-like manner and magnetized. The particle based microrobot was shown in a previous study to have sufficient rigidity to maintain their structures under strong magnetic forces [35]. A representative example of a three-bead microrobot is shown in Fig. 1a. According to *Happel* and *Brenner*, an object with two symmetry planes can produce a forward propulsive force when rotated by an external torque [37]. Therefore, this microrobot is actuated by rotating magnetic field enabling the body of the microrobot to rotate. This rotational motion converts the torque into translational force. In addition, the static magnetic field allows the heading of an achiral microrobot to keep forward. As a result, the translation direction is perpendicular to the rotating magnetic field as indicated in Fig. 1b.

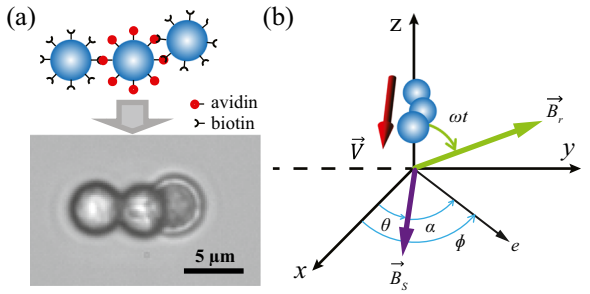

Fig. 1 Fabrication and schematic of the particle based microswimmer. **a** Example of a three-bead microswimmer created by avidin-biotin linkage and magnetic attraction, **b** Schematic of the coordinate frame for kinematic modeling and feedback control

2.2 Magnetic control system

To achieve an effective control method for the microrobots, we utilized a combination of static and rotating magnetic fields. The magnetic fields are supplied by a 3D approximate Helmholtz coil system. The static magnetic field is used to adjust the orientation of the microrobot toward the desired direction and the rotating magnetic field is used to provide the propulsive motion to the microrobot. Thus, the resultant magnetic field generated from three pairs of electromagnetic coils results in the controllability of the achiral microrobots in the 2D plane. The resultant magnetic field is described as

$$\mathrm{B} = \begin{bmatrix} -B_s\cos(\theta) + B_r\sin(\theta)\cos(\omega t) \\ B_s\sin(\theta) + B_r\cos(\theta)\cos(\omega t) \\ B_r\sin(\omega t) \end{bmatrix} \quad (1)$$

where B_r is the maximum amplitude of the rotating magnetic field, B_s is the magnitude of the static magnetic field, ω is the rotational frequency of the field, θ is the direction of rotation, and t is time. The schematic for Eq. (1) is illustrated in Fig. 1b. The plane of the rotating field and the perpendicular static field rotate synchronously are based on the microrobot's orientation θ. The heading angle of swimming motion and the static field direction can be expressed as

$$\hat{n} = [-\cos(\theta)\ \ \sin(\theta)\ \ 0]^T \quad (2)$$

National Instrument (NI) data acquisition (DAQ) controllers were used to provide sinusoidal signals to three power supplies that powered the x, y, z coils. The input signals were based on Eq. (1). In experiments, the rotation frequency ω and the angle θ were determined by the feedback controller to modulate the swimming velocity and control the heading.

2.3 Experimental system setup

The control system consists of an electromagnetic coil system, three power supplies (Kepco), DAQ board (NI), a computer, an inverted microscope (Leica), and a camera (Point Grey) as shown in Fig. 2. The electromagnetic coil system has three pairs of coils arranged in Helmholtz configuration. Each coil pair is connected to a power supply that is programmable and controlled by the computer through the DAQ board. The center has 5 mT when 1 Amp of current is passing through two pairs of coils. A LabVIEW interface incorporates camera and magnetic field control; this allows us to perform real-time image processing for feedback control of the microrobot. The camera records at 30 fps and the sampling time for the image processing and feedback control is 0.2 s due to the limitation of the system. The static obstacles were fabricated by traditional photolithography with SU-8 2150 and have a thickness of 260 μm. As a result, we could locate the static obstacles inside of the closed chamber. The chamber was filled with motility buffer (0.01 M potassium phosphate, 0.067 M sodium chloride, 10^{-4} M ethylendediaminetetraacetic acid (EDTA), 0.01 M glucose, pH 7.4). The experiment chamber was installed in the middle of electromagnetic coil system. For feedback control and path planning, the achiral microrobot was localized by image processing and the rest of objects excluding the target achiral microrobot were detected as obstacles in the binary image results. The achiral microrobots were swimming above 20 μm height from the bottom glass surface using NaCl solution that minimize vertical drift from sedimentation or buoyancy.

3 Motion planning for achiral microrobots

The motion planning has two main algorithms for autonomous navigation in static obstacle; The first algorithm is to control the locomotion of the microrobot for following the generated path using feedback control [38]. The second algorithm is to provide the microrobot with the path trajectory using the gradient method.

3.1 Kinematic model

The kinematics of the achiral microrobot are similar to that of a unicycle because the heading angle and velocity of the achiral microrobot is enable to be controlled by setting direction and rotation frequency of electromagnetic fields, respectively [39]. The achiral microrobot's kinematic model can be expressed by the non-linear model as follows:

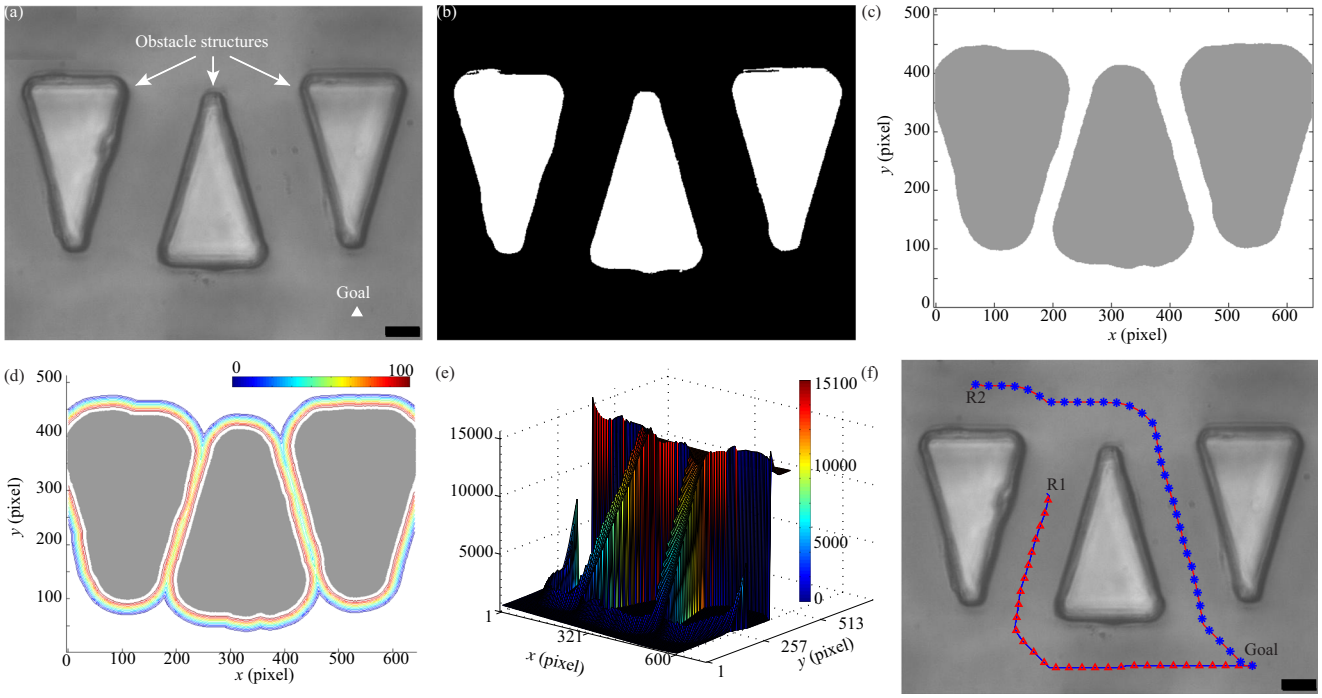

Fig. 2 System setup for experiment. The three power supplies connected to an electromagnetic coil system. The DAQ device, which is connected to the power supplies, allows for precise control over the direction and magnitude of the magnetic field. The microscope and camera provide visual feedback and video recording. All of the operation parameters can be controlled using the LabVIEW program

$$\begin{aligned} \dot{x}(t) &= v(u_1(t))\cos(\theta(t)) \\ \dot{y}(t) &= v(u_1(t))\sin(\theta(t)) \\ \dot{\theta}(t) &= u_2(t) \end{aligned} \tag{3}$$

where v is the forwarding velocity of the rotating microrobot, $u_1(t)$ is the rotation frequency and $u_2(t)$ is the turning rate of the rotating magnetic field. It was observed that the swimming speed, v, has a liner relationship with the rotation frequency, $u_1(t)$ in [35]. In previous work, the average velocity profiles were obtained using 30 random samples for each frequency (i.e., 1 Hz, 2 Hz, ⋯, 8 Hz). The high frequency of the rotating magnetic field enables a microrobot to rotate its own body at a faster rate. The velocity function in the modeling of the achiral microrobot can be expressed by the linearization of the curve fitting line using the coefficient, $\hat{p}_1$. As a result, we can obtain the stochastic model for the achiral microrobot described as

$$\begin{aligned} \dot{x}(t) &= \hat{p}_1 u_1(t)\cos(\theta(t)) \\ \dot{y}(t) &= \hat{p}_1 u_1(t)\sin(\theta(t)) \\ \dot{\theta}(t) &= u_2(t) \end{aligned} \tag{4}$$

The p_1 was derived from experiment and has a value of 0.428 [35].

3.2 Motion planning

There have been many studies about the motion control for a nonholonomic unicycle-like model. Model-based control methods such as MPC are applied for nonholonomic robots to follow paths [31, 40]. Other methods use sampling-based motion planning approaches such as, the Probabilistic Road Map (PRM) and RRT. To guide the microrobot from present position towards a target position, we utilize a well-known Lyapunov function, which states that certain parameters are zero when the desired goal position and orientation are reached, i.e. when $e = \alpha = \phi = 0$. The feedback control system is designed using the kinematics Eq. (3) and $e = \sqrt{x^2 + y^2}$ which is the error between the position of a microrobot and the target position. Based on this, the time derivative of the error distance vector e can be written as

$$\dot{e}(t) = \frac{x\dot{x} + y\dot{y}}{e} = \frac{xv(u_1(t))\cos(\theta) + yv(u_1(t))\sin(\theta)}{e} \tag{5}$$

where θ is the achiral microrobot's heading angle (Fig. 1b). We define the α as the difference of angle between the microrobot's heading angle and the angle to the desired target position ($\alpha = \phi - \theta$), and $\phi = \tan^{-1}(y/x)$. Letting $-x = e\cos(\alpha + \theta)$ and $-y = e\sin(\alpha + \theta)$, we finally have [41].

$$\begin{aligned}\dot{e}(t) &= -p_1 u_1(t)\cos(\alpha(t)) \\ \dot{\alpha}(t) &= -u_2(t) + p_1 u_1(t)\frac{\sin(\alpha(t))}{e(t)} \\ \dot{\phi}(t) &= p_1 u_1(t)\frac{\sin(\alpha(t))}{e(t)}\end{aligned} \tag{6}$$

To avoid the occurrence of a singularity, these equations are valid only for non-zero values of distance errors e. By applying the Lyapunov function [39] as

$$V(t) = \frac{\lambda}{2}e^2 + \frac{1}{2}\alpha^2(t) + \frac{h}{2}\phi^2(t) \tag{7}$$

where $\lambda > 0$, $k > 0$, $h > 0$, and from the condition $\dot{V} < 0$, the following control law can be built for general PID control

$$\begin{aligned}u_1(t) &= \gamma e(t)\cos(\alpha(t)) \\ u_2(t) &= k\alpha(t) + p_1\gamma\frac{\cos(\alpha(t))\sin(\alpha(t))}{\alpha(t)}(\alpha(t) + h\phi(t))\end{aligned} \tag{8}$$

where γ, k, and h are tunable parameter at the spatiotemporal scale of μm/s. By control input u_1 and u_2, the microrobot can be located in any position in space. In this paper, we simplified the controller for pure pursuit because of the limitation of system setup in terms of input frequency of rotating magnetic field. Hence, the control inputs are $u_1(t) = C$, $u_2(t) = k\alpha(t)$. For $u_1(t)$, it was fixed with a constant value to generate a consistent frequency of magnetic field depending on motion of the achiral microrobots. In case of $u_2(t)$, the $k\alpha(t)$ is only left. The performance of this condition was shown in [41, 42]. The $e(t)$ is calculated between the current position of the microrobot and the current target waypoint. The reminded tunable parameter, k, was determined by experimental testing.

3.3 Path planning using gradient method

To ensure that microrobots approach the goal position without collision or loss of controllability, a reliable and safe path planning method should be utilized. In particular, if achiral microswimmers swim near a wall, they can easily be stuck to the surface of the wall. Once attached to the wall surface, microrobot rotation becomes hindered, making it difficult to detach under the rotating magnetic fields. During experimentation, this only occurred when we had our microswimmers swim in close proximity to the wall.

In the map, one grid of the map is 1 pixel × 1 pixel. Using the gradient method, all grids of the empty space have a cost value which represents the distance from the goal and the distance from the close obstacles using Eq. (9)

$$F(P) = \sum_i I(p_i) + \sum_i A(p_i, p_{i+1}) \tag{9}$$

where I is the intrinsic cost function, giving high cost assignment when in proximity to an obstacle. A is the path length function from the goal to the current point on the map. Therefore, the generated trajectory has a minimum cost path to the goal position [36]. In addition, the local minima problem can be resolved. The Configuration space (C-space) is utilized to ensure a safe distance between the obstacles and microrobots by expanding the obstacles. This path planning requires the whole information of environment, where Eq. (9) should be recalculated when the goal position is changed.

There are mainly three computation steps to generate the path to the goal position. First step is to generate C-space using a grid-map that is converted from a real image through microscope (Fig. 3a, b). The size of the microrobots was regarded as a radius for the C-space, as shown in Fig. 3c. This C-space is helpful to extract the empty space regarding the motion of the microrobot because the microrobot can be represented by one dot. Then, the intrinsic cost is computed for the areas not occupied by the C-space. The intrinsic cost represents potential field of danger. As indicated in Fig. 3d, the closer the area is to the obstacles, the higher the cost is. Finally, path cost from the selected goal position is calculated. The path cost accounts for the distance from the goal and the intrinsic cost. Thus, the empty space on the grid-map has different values. This allows the microrobot to approach the goal position no matter where the microrobot is initially located on the map as illustrated in Fig. 2e. This path cost helps microrobots to avoid areas where local minima problems exist. In addition, the generated path

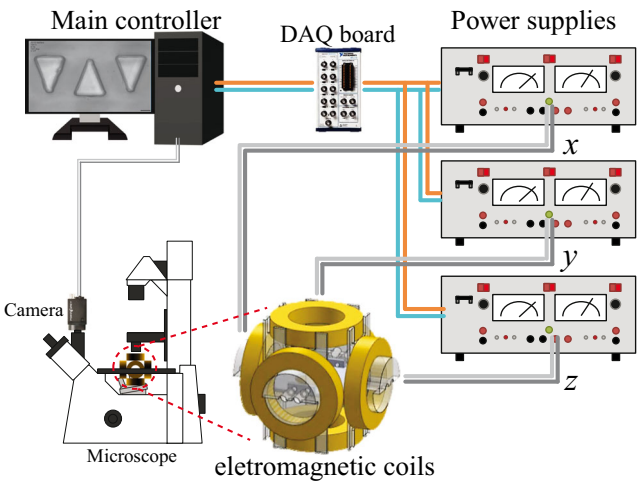

Fig. 3 Gradient path planning for particle based microrobots. **a** Captured image from a camera with a manually chosen goal, **b** Binary image processing for path planning (white areas represent objects), **c** C-space on grid map using binary image (white areas represent free space for the achiral microrobot), **d** Contour graph of intrinsic potential field using C-space, **e** Path cost on whole area from a goal position, **f** Paths from two different initial locations (R1, R2), the scale bar represents 20 μm

provides the microrobot with the distance from the wall to prevent the wall effect and pass through the obstacle. After the path is generated, the way points of the path are chosen depending on the distance between the current position of the microrobot and the points among the path. During the experiments, the way point, which was ahead of the robot, with a certain distance, was chosen continuously once the microrobot reached the previous way point.

4 Discussion

The k, in Eq. (8), was 5 for all experiments because of the sampling time frequency. Through the gradient path planning algorithm, a series of waypoint is generated which defines a path from the microrobot's current position to the goal position. Once the path is generated, the feedback controller guides the microrobot through the waypoints. In experiments, we demonstrated two different environmental maps to demonstrate the reliability of the path planning algorithm and the robustness of the feedback control system. For the path following, the certain distant way point enabled the microrobot to follow the path with less error.

4.1 Motion control for following path

A microrobot with three beads was used in this experiment. The environmental map features three triangular obstacles with an interspatial dimension of 35 μm. The initial position of the microrobot was at the left top corner and the goal was located on the bottom right (Fig. 4a). There were two ways to approach the goal. As a result of gradient path planning, the pathway on the right between obstacle 2 and obstacle 3 was chosen as the minimal cost path as shown in Fig. 4a. The control inputs for u_2 are indicated in Fig. 4b. As shown in Fig. 4b, the α has the average value of 0.35, meaning the heading angle of the microrobot was controlled to follow the path with stable heading control during most of time.

Using gradient path planning, the microrobot was able to choose the minimal cost path between the two diverged ways at 15.2 s. Then, the achiral microrobot could swim a safe distance from the two static obstacles until 60.8 s, where it was no longer in danger of collision. Finally, it approached the goal position with the path at 73 s. In terms of controller, we set the frequency as 10 Hz, and the velocity is the average of 2.2 μm/s. However, the velocity fluctuated as shown in Fig. 4b due to uncertainties and environmental factors such as Brownian motion. It is observed that the target waypoints maintained within 4 μm distant from the achiral microrobot.

4.2 Comparison of two different achiral microrobots

In this experiment, two different microrobots were demonstrated to follow the same path in the same environment. The first microrobot had two beads and the second one had three beads. Both microrobots started from the top right position and reached the bottom right goal. To compare the result trajectories, the control input $u_1(t)$ had 10 Hz that represents the frequency of magnetic field.

As shown in Fig. 5, the two microrobots both reached the target position with minimal deviation from the computed path. In general, a longer thread of beads of microrobots generates higher velocity under the same frequency of the rotating magnetic field [42]. However, higher velocities increase the probability of collision with static obstacles. In the case of three bead based microrobot, it took 97 s to approach the goal location. On the other hand, the two beads microrobot swam during 270 s. In addition, comparing to the previous

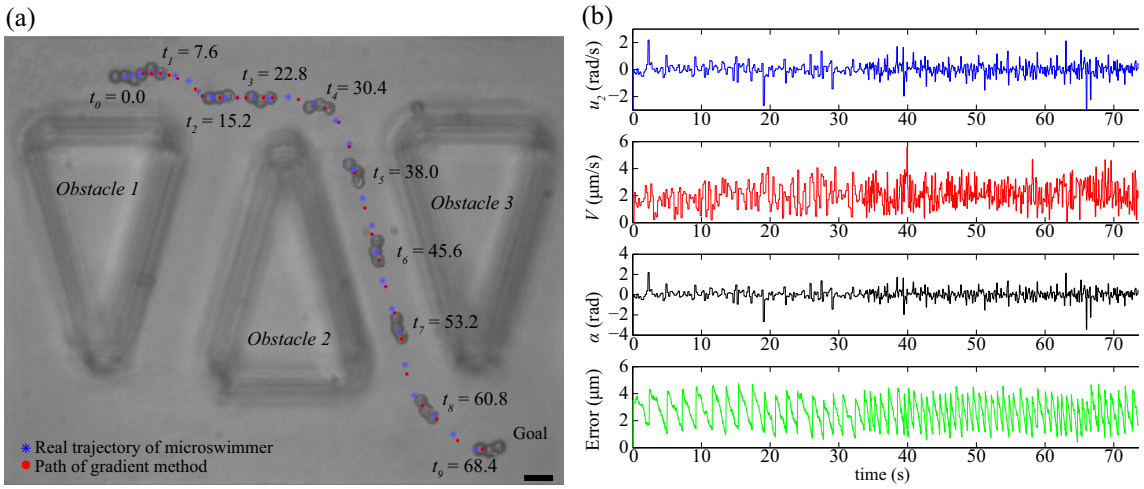

Fig. 4 Motion planning experiment result using a three-bead microswimmer. **a** Resultant trajectory of microswimmer with gradient path, **b** Control input values in feedback controller, velocity of the microswimmer, angle different angle between the heading angle of the microswimmer and a target waypoint, and error distance between real position of microswimmer and path. The scale bar is 20 μm

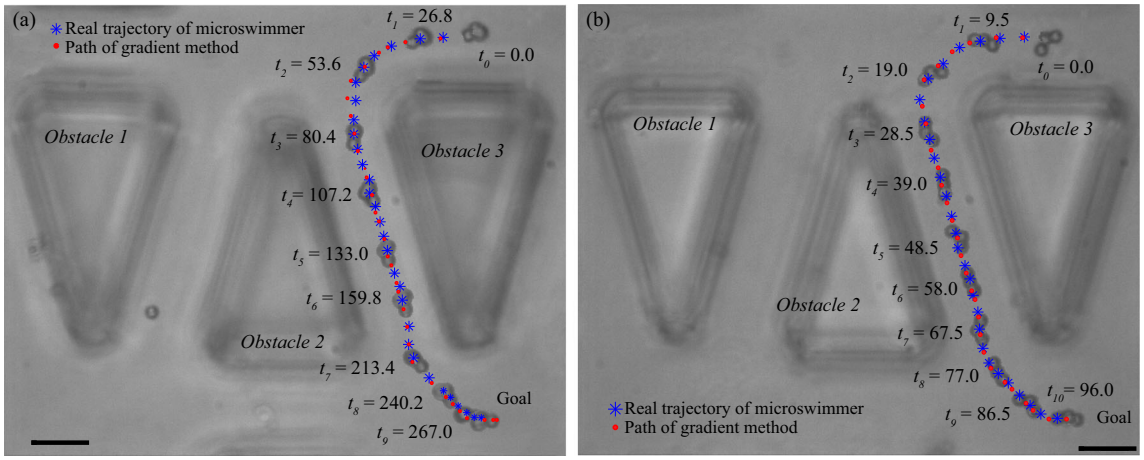

Fig. 5 Two experimental results using the same path in the same environment. **a** The path following motion using a two-bead microswimmer, **b** The path following motion using a three-bead microswimmer. The scale bar represents 35 μm

experiments, the microrobots need to complete a sharp turn in order to enter the valley between obstacle 2 and 3 (t_1~t_4 in Fig. 5). As a demonstration of the robustness of the navigation system, the microrobots safely completed the turn by moving around the corner of obstacle 3 and passed through the valley without collision. This result indicates that the motion planning is reliable and repeatable using different microrobots.

4.3 Path following in narrow channel

When a particle based microrobot rotates, its effective size (length and radius) increased. An analogy is when a simple rod rotates fast enough, its effective coverage area is shaped like a disk. Thus, when we consider a microrobot rotating and swimming near a wall, we have to consider its effective size in order to avoid collision. To demonstrate the robust control of our motion planning, we placed a microrobot in narrow pathways with a width of 25 μm. The microrobot used in this experiment had an effective length and radius of 15 μm and 8 μm respectively; this was a four-bead microswimmer. When gradient path planning was applied, the narrowness of the pathway had to be considered and could not inflate the obstacles to a degree where the *C*-space would block paths to the goal. Thus, the *C*-space was kept to a minimum, which in turn increased the risk of collision if the microrobot deviated too much from the intended path. The generated path and the trajectory of the microrobot are shown in Fig. 6. While the microrobot was controlled by motion planning algorithm, the closest distance between the microrobot's centroid and the obstacles are evaluated as explained in Fig. 7. When the microrobot entered from one channel to the other channel, it turned with safe distance around the corner between 63 s and 84 s. As a result, the microrobot maintained an average 10 μm distant from the obstacles while it moved in the narrow channel. Through this experiment, we have proved that the achiral microrobot is able to swim with rotating motion in the narrow channel under autonomous control.

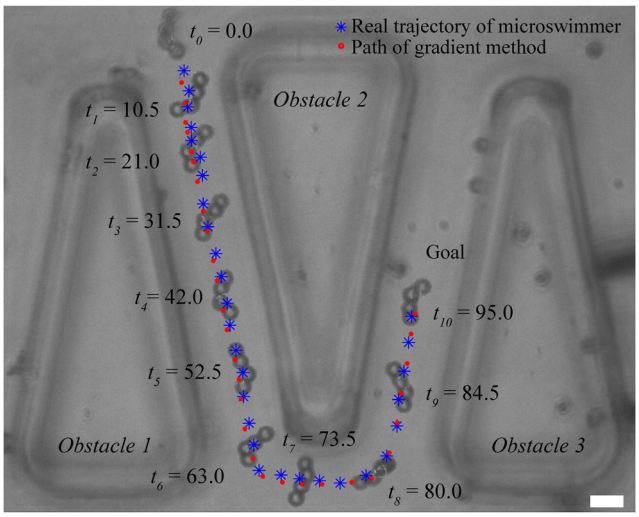

Fig. 6 Experiment result in the narrow channel environment. The scale bar represents 10 μm

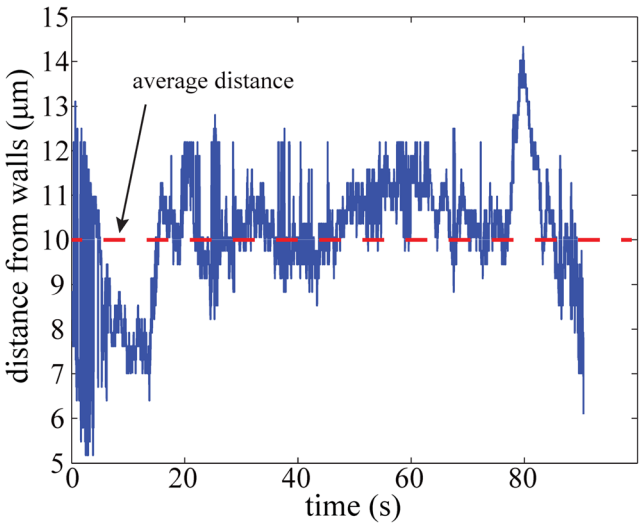

Fig. 7 Closet distance between the center of mass and the wall of obstacle

5 Conclusion

We demonstrated motion planning in environments where multiple static obstacles were placed. Our motion planning approach combined gradient path planning and feedback control to successfully guide microrobots to the goal positions. This was shown in experiments where microrobots were able to follow the generated paths with high accuracy in various environments. The implementation of gradient path planning allowed us to compute the minimal cost path among several pathways. This autonomous navigation system demonstrated the controllability of the particle based microrobots and their ability reach the target positions without collision. Notably, the microrobots were able to move through very narrow pathways. This navigation strategy for microrobots will be useful to guide magnetic microrobots through confined spaces, thus, increasing the precision for manipulation in small scales.

Acknowledgements We thank Prof. Dejan Milutinović and Prof. Jongeun Choi for their contribution in developing the kinematic model. This work was funded by National Science Foundation (CMMI#1712096).

References

1. Purcell EM (1977) Life at low Reynolds number. Am J Phys 45:3–11
2. Zhang L, Abbott JJ, Dong L, Kratochvil BE, Bell D, Nelson BJ (2009) Artificial bacterial flagella: fabrication and magnetic control. Appl Phys Lett 94:064107
3. Zhang L, Ruh E, Grützmacher D, Dong L, Bell DJ, Nelson BJ et al (2006) Anomalous coiling of SiGe/Si and SiGe/Si/Cr helical Nanobelts. Nano Lett 6:1311–1317
4. Tottori S, Zhang L, Qiu F, Krawczyk KK, Franco-Obregón A, Nelson BJ (2012) Magnetic helical micromachines: fabrication, controlled swimming, and cargo transport. Adv Mater 24:811–816
5. Ghosh A, Fischer P (2009) Controlled propulsion of artificial magnetic nanostructured propellers. Nano Lett 9:2243–2245
6. Cheang UK, Roy D, Lee JH, Kim MJ (2010) Fabrication and magnetic control of bacteria-inspired robotic microswimmers. Appl Phys Lett 97:213704
7. Temel FZ, Yesilyurt S (2011) Magnetically actuated micro swimming of bio-inspired robots in mini channels. in *International Conference on Mechatronics*, Istanbul, Turkey:342–347
8. Gao W, Feng X, Pei A, Kane CR, Tam R, Hennessy C et al (2013) Bioinspired helical microswimmers based on vascular plants. Nano Lett 14:305–310
9. Kim DH, Cheang UK, Kohidai L, Byun D, Kim MJ (2010) Artificial magnetotactic motion control of Tetrahymena pyriformis using ferromagnetic nanoparticles: a tool for fabrication of microbiorobots. Appl Phys Lett 97:173702
10. Steager EB, Sakar MS, Kumar V, Pappas GJ, Kim MJ (2011) Electrokinetic and optical control of bacterial microrobots. J Micromech Microeng 21:035001
11. Leoni M, Kotar J, Bassetti B, Cicuta P, Lagomarsino MC (2009) A basic swimmer at low Reynolds number. Soft Matter 5:472–476
12. Mori N, Kuribayashi K, Takeuchi S (2010) Artificial flagellates: analysis of advancing motions of biflagellate micro-objects. Appl Phys Lett 96:083701
13. Peyer KE, Zhang L, Nelson BJ (2013) Bio-inspired magnetic swimming microrobots for biomedical applications. Nano 5:1259–1272
14. Sakar MS, Steager EB, Kim DH, Kim MJ, Pappas GJ, Kumar V (2010) Single cell manipulation using ferromagnetic composite microtransporters. Appl Phys Lett 96:043705
15. Khalil ISM, Keuning JD, Abelmann L, Misra S (2012) Wireless magnetic-based control of paramagnetic microparticles. In: 2012 4th IEEE RAS & EMBS international conference on biomedical robotics and biomechatronics (BioRob), pp 460–466
16. Belharet K, Folio D, Ferreira A (2014) Study on rotational and unclogging motions of magnetic chain-like microrobot. In: 2014 IEEE/RSJ international conference on intelligent robots and systems, pp 834–839
17. Khalil ISM, Abelmann L, Misra S (2014) Magnetic-based motion control of paramagnetic microparticles with disturbance compensation. IEEE Trans Magn 50(10):1
18. Chowdhury S, Jing W, Jaron P, Cappelleri DJ (2015) Path planning and control for autonomous navigation of single and multiple magnetic mobile microrobots, p V004T09A040
19. Chowdhury S, Jing W, Cappelleri D (2016) Towards independent control of multiple magnetic mobile microrobots. Micromachines 7:3
20. Chowdhury S, Johnson BV, Jing W, Cappelleri DJ (June 01 2017) Designing local magnetic fields and path planning for independent actuation of multiple mobile microrobots. Journal of Micro-Bio Robotics 12:21–31
21. Hu S, Sun D, Feng G (2010) Dynamics analysis and closed-loop control of biological cells in transportation using robotic manipulation system with optical tweezers. In: 2010 I.E. Conference on automation science and engineering (CASE), pp 240–245
22. Tanaka Y, Kawada H, Hirano K, Ishikawa M, Kitajima H (2018) Automated manipulation of non-spherical micro-objects using optical tweezers combined with image processing techniques. Opt Express 16: 15115–15122
23. Banerjee AG, Pomerance A, Losert W, Gupta SK (2010) Developing a stochastic dynamic programming framework for optical tweezer-based automated particle transport operations. IEEE Trans Autom Sci Eng 7:218–227
24. Ju T, Liu S, Yang J, Sun D (2011) Apply RRT-based path planning to robotic manipulation of biological cells with optical tweezer. In: 2011 International conference on mechatronics and automation (ICMA), pp 221–226
25. Cappelleri DJ, Fatovic M, Shah U (2011) Caging micromanipulation for automated microassembly. In: 2011 I.E. International conference on robotics and automation (ICRA), pp 3145–3150
26. Belharet K, Folio D, Ferreira A (2010) Endovascular navigation of a ferromagnetic microrobot using MRI-based predictive control. In: 2010 IEEE/RSJ International conference on intelligent robots and systems (IROS), pp 2804–2809
27. Kim DH, Brigandi S, Julius AA, Min Jun K (2011) Real-time feedback control using artificial magnetotaxis with rapidly-exploring random tree (RRT) for Tetrahymena pyriformis as a microbiorobot. In: 2011 I.E. International conference on robotics and automation, pp 3183–3188
28. Pieters R, Tung H-W, Charreyron S, Sargent DF, Nelson BJ (2015) RodBot: a rolling microrobot for micromanipulation. In: 2015 I.E. International conference on robotics and automation (ICRA), pp 4042–4047
29. Pieters R, Lombriser S, Alvarez-Aguirre A, Nelson BJ (2016) Model predictive control of a magnetically guided rolling microrobot. IEEE Robotics and Automation Letters 1:455–460
30. Scheggi S, Misra S (2016) An experimental comparison of path planning techniques applied to micro-sized magnetic agents. In:

2016 international conference on manipulation, automation and robotics at small scales (MARSS), pp 1–6
31. Soetanto D, Lapierre L, Pascoal A (2003)Adaptive, non-singular path-following control of dynamic wheeled robots. In: 42nd IEEE International conference on decision and control (IEEE Cat No03CH37475), vol 2, pp 1765–1770
32. Jiang Z-P, Lefeber E, Nijmeijer H (2001) Saturated stabilization and tracking of a nonholonomic mobile robot. In: Systems & control letters, vol 42, pp 327–332
33. Belharet K, Folio D, Ferreira A (2013) Simulation and planning of a magnetically actuated microrobot navigating in the arteries. IEEE Trans Biomed Eng 60:994–1001
34. Xu T, Hwang G, Andreff N, Régnier S (2015) Planar path following of 3-D steering scaled-up helical microswimmers. IEEE Trans Robot 31:117–127
35. Cheang UK, Milutinović D, Choi J, Kim MJ (2014) Towards model-based control of achiral microswimmers. In: Presented at the the ASME dynamic systems and control conference, TX, USA
36. Konolige K (2000) A gradientmethod for realtime robot control. In: 2000 IEEE/RSJ Proceedings in international conference on intelligent Robots and Systems (IROS 2000) (Cat. No00CH37113), vol 1, pp 639–646
37. Happel J, Brenner H (1965) Low Reynolds number hydrodynamics: with special applications to particulate media, vol 1, Springer
38. Siciliano B, Sciavicco L, Villani L, Oriolo G (2010) Robotics: modelling, planning and control. Springer Science & Business Media
39. Aicardi M, Casalino G, Bicchi A, Balestrino A (1995) Closed loop steering of unicycle like vehicles via Lyapunov techniques. IEEE Robot Autom Mag 2:27–35
40. Farrokhsiar M, Pavlik G, Najjaran H (2013) An integrated robust probing motion planning and control scheme: a tube-based MPCapproach. Robot Auton Syst 61:1379–1391
41. Cheang UK, Kim H, Milutinović D, Choi J, Kim MJ (2017) Feedback control of an achiral robotic microswimmer. J Bionic Eng 14:245–259
42. Cheang UK, Meshkati F, Kim H, Lee K, Fu HC, Kim MJ (2016) Versatile microrobotics using simplemodular subunits, vol 6, p 30472